Response of the Pacific and Atlantic oceans to interannual variations in net atmospheric freshwater

Boyin Huang and Vikram M. Mehta
Center for Research on the Changing Earth System, Columbia, Maryland, USA

Received 1 December 2004; revised 18 March 2005; accepted 24 March 2005; published 13 August 2005.

[1] The response of the Pacific and Atlantic Oceans to net atmospheric freshwater (evaporation minus precipitation (EmP)) between 1988 and 2000 was studied using a global ocean general circulation model developed in the Massachusetts Institute of Technology. Evaporation estimates from the Goddard Satellite Surface Turbulent Fluxes and precipitation estimates from the Global Precipitation Climatology Project were used. Model simulations showed that the spatial distribution of the average sea surface salinity (SSS) changes during the 1988–2000 period resembled that of average EmP changes, because SSS changes were primarily associated with anomalous vertical mixing forced by the anomalous EmP. The spatial distribution of average near-surface temperature anomalies, however, was different from those of average EmP and SSS anomalies. Analyses indicated that temperature changes in the subtropical North and South Pacific resulted from anomalous heat advection which, in turn, resulted from changes in the subtropical gyre circulations. Temperature changes in the tropical Pacific were associated with anomalous heat advection due to changes in the South Equatorial Current (SEC). Furthermore, the changes in the subtropical gyres and the SEC resulted largely from anomalous EmP in the subtropical Pacific. Temperature changes in the Atlantic, however, were largely associated with vertical mixing changes due to anomalous EmP. Observed interannual variations of SSS in the Western Pacific Warm Pool were simulated successfully. A large difference between simulated and observed SSS, however, was found in the central equatorial Pacific. Simulated SSS and temperature varied at interannual and longer timescales in most of the Pacific and Atlantic Oceans. Large changes in SSS and temperature due to anomalous EmP in the Pacific and Atlantic strongly suggest that EmP variability can play an important role in ocean and climate variabilities at interannual and longer timescales.

Citation: Huang, B., and V. M. Mehta (2005), Response of the Pacific and Atlantic oceans to interannual variations in net atmospheric freshwater, *J. Geophys. Res.*, *110*, C08008, doi:10.1029/2004JC002830.

1. Introduction

[2] Interactions between sea surface temperature (SST) and the atmosphere can cause climate variability at interannual and longer timescales. The SST can be affected by many factors such as ocean heat advection [see, e.g., *Miller et al.*, 1994; *Deser et al.*, 1996; *Gu and Philander*, 1997; *Lysne et al.*, 1997; *Huang and Liu*, 2001, 2002], surface heat flux [see, e.g., *White and Barnett*, 1972; *Cayan*, 1992; *Lau and Nath*, 1996; *Masuda*, 2002], and Rossby waves [see, e.g., *Jacobs et al.*, 1994]. Many studies indicated that changes in both ocean heat advection and surface heat flux can be associated with changes in surface winds [*Cayan*, 1992; *Lau and Nath*, 1996; *Huang and Liu*, 2001, 2002], because upper-ocean currents are driven largely by winds and wind speed is one of the fundamental factors affecting latent (evaporation) and sensible heat fluxes. Winds, however, are highly coupled with SST at tropical [*Walker*, 1924; *Bjerknes*, 1969; *Philander*, 1990; *Liu and Huang*, 1997] and subtropical [*Latif and Barnett*, 1994, 1996; *Giese and Carton*, 1999] latitudes. As this brief summary indicates, studies of interactions between the oceans and the atmosphere via surface heat flux and wind stress have a long history. Possible responses of the oceans to net atmospheric freshwater (evaporation minus precipitation (EmP)), however, have attracted attention only recently [see, e.g., *Schneider and Barnett*, 1995; *Vialard and Delecluse*, 1998a, 1998b; *Murtugudde and Bussalacchi*, 1998; *Yang et al.*, 1999; *Perigaud et al.*, 2003; *Huang and Mehta*, 2004; *Fedorov et al.*, 2004].

[3] Our previous study using the Massachusetts Institute of Technology (MIT) ocean general circulation model (OGCM) indicated that the SST changed significantly due to anomalous EmP [*Huang and Mehta*, 2004] in the Indo-Pacific Warm Pool (IPWP) during the 1988 to 2000 period. This SST change may play an important role in climate variability at interannual and longer timescales. Therefore

0148-0227/05/2004JC002830$09.00

we hypothesized that anomalous EmP can have large impacts on SST at interannual and longer timescales by changes in basin-scale ocean circulations and heat transports due to anomalous EmP forcing in the Pacific and Atlantic oceans. Specifically, we address the following questions in the present study: What is the response of the Pacific and Atlantic oceans to interannual variability of the EmP? What are the mechanisms of the response? These questions are addressed with the MIT OGCM forced by monthly evaporation and precipitation estimates, based on satellite-measured infrared and microwave radiances, for the 1988–2000 period.

[4] Observed evaporation and precipitation estimates are described briefly in section 2. The MIT OGCM and experiment design are described in section 3. The time-averaged responses of the upper Pacific and Atlantic oceans are described in section 4. Interannual variabilities of the Pacific and Atlantic oceans are described in section 5. Sensitivities of oceanic responses to regional anomalous EmP in the Pacific and to the model SST boundary condition are discussed in section 6. The results are summarized in section 7.

2. Satellite-Based Net Atmospheric Freshwater Estimates

[5] Monthly precipitation estimates used in this study are from the Global Precipitation Climatology Project (GPCP) version 2 [*Huffman et al.*, 1997] from January 1988 to December 2000. Monthly evaporation estimates used in this study are from the Goddard Satellite Surface Turbulent Fluxes version 2 (GSSTF2) [*Chou et al.*, 1997] for the same period. The GSSTF2 evaporation estimates are available on a 1° longitude × 1° latitude grid over the oceans from 50°S to 60°N whereas the GPCP version 2 precipitation estimates are available on a 2.5° longitude × 2.5° latitude grid from 90°S to 90°N. Monthly evaporation and precipitation estimates were interpolated to the OGCM grid and monthly EmP was calculated on the OGCM grid.

[6] Figure 1a shows the average EmP between 1988 and 2000. Consistent with other observations, evaporation exceeded precipitation in the subtropical North Pacific and North Atlantic between 10°N and 35°N, the southeast South Pacific east of the 180° longitude, the southwest South Pacific east of Australia, and the South Atlantic. In contrast, precipitation exceeded evaporation in the Inter-Tropical Convergence Zone in the North Pacific near 8°N and in the North Atlantic near 5°N, in the South Pacific Convergence Zone north of 10°S and west of 160°W, and in the higher latitudes of the North Pacific and North Atlantic north of 30°N.

[7] Figure 1b shows averaged EmP anomaly relative to 1988 (average of 1989–2000 minus average of 1988). The reason for using 1988 as the reference year was to ensure a smooth evolution of EmP forcing in our model experiments. This is described further in the next section. It is clear that there was a large, in magnitude and areal extent, negative EmP anomaly in the equatorial Pacific between 10°S and 10°N east of 150°E (1.0 m yr^{-1}). A positive EmP anomaly existed during this period in the subtropics of the North Pacific between 15°N and 45°N (0.75 m yr^{-1}), in the subtropics of the South Pacific between 10°S and 45°S (1.0 m yr^{-1}), and in the tropical Atlantic between 10°S and 15°N (0.5 m yr^{-1}).

3. MIT OGCM and Experiment Design

[8] The OGCM developed in the MIT [*Marshall et al.*, 1997; *Huang et al.*, 2003] was used in this study as in some of our previous studies [see, e.g., *Huang and Mehta*, 2004]. The OGCM domain is from 80°S to 90°N and from 0° longitude to 360° longitude with a realistic topography. Briefly, the OGCM's latitudinal resolution varies from 0.4° near the equator to 2° at and poleward of 20°N and 20°S, and the longitudinal resolution is 2°. The vertical resolution is 10 to 50 m above 400 m depth, and 75 to 250 m between 400 and 1000 m depths. Vertical diffusivity and viscosity are calculated from the K-profile parameterization (KPP) [*Large et al.*, 1994]. The vertical mixing associated with diffusivity and viscosity is calculated using an implicit scheme. The *Shapiro* [1970] filter is applied to both zonal and meridional currents every 12 hours with a damping timescale of 1 hour.

[9] As in the work of *Huang and Mehta* [2004], the OGCM was spun up for 200 years from a motionless initial state of annual temperature from *Levitus and Boyer* [1994] and salinity from *Levitus et al.* [1994]. During the spinup, the OGCM was forced by monthly wind stress from *Hellerman and Rosenstein* [1983]. The model sea surface salinity (SSS) was forced by monthly EmP of 1988, which was to ensure a smooth EmP transition when simulation experiments were started from 1988 to 2000. The SSS was restored to the monthly climatology of *Levitus and Boyer* [1994] poleward of 55°S and 65°N with a damping timescale of 60 days, since the satellite-based EmP estimates were available only between 55°S and 65°N.

[10] The model SST was forced by a mixed surface boundary condition during the spinup. This consisted of monthly net heat flux from the Comprehensive Ocean Atmosphere Data Set (COADS) [*da Silva et al.*, 1994], and a restoring of SST to monthly climatology from *Levitus and Boyer* [1994] with a damping timescale of τ_1 (10 days; equivalent to 50 Wm^{-2} K^{-1}):

$$dT/dt = Q_{COADS}/\rho c_p \Delta z_1 + (SST - T)/\tau_1. \quad (1)$$

The monthly net heat flux into the model ocean was diagnosed after the spinup. The diagnosed net heat flux included the original COADS net heat flux and the SST restoring term,

$$Q_{Model} = Q_{COADS}/\rho c_p \Delta z_1 + (SST - T)/\tau_1. \quad (2)$$

We used this diagnosed net heat flux as a flux boundary condition that allows an SST perturbation to evolve according to ocean thermodynamics and dynamics,

$$dT/dt = Q_{Model}. \quad (3)$$

[11] Two experiments (Table 1) were designed first: a control (CTR) experiment and a perturbation (PTB) experiment. Monthly EmP of 1988 was used in CTR, and monthly EmP from 1988 to 2000 was used in PTB. CTR

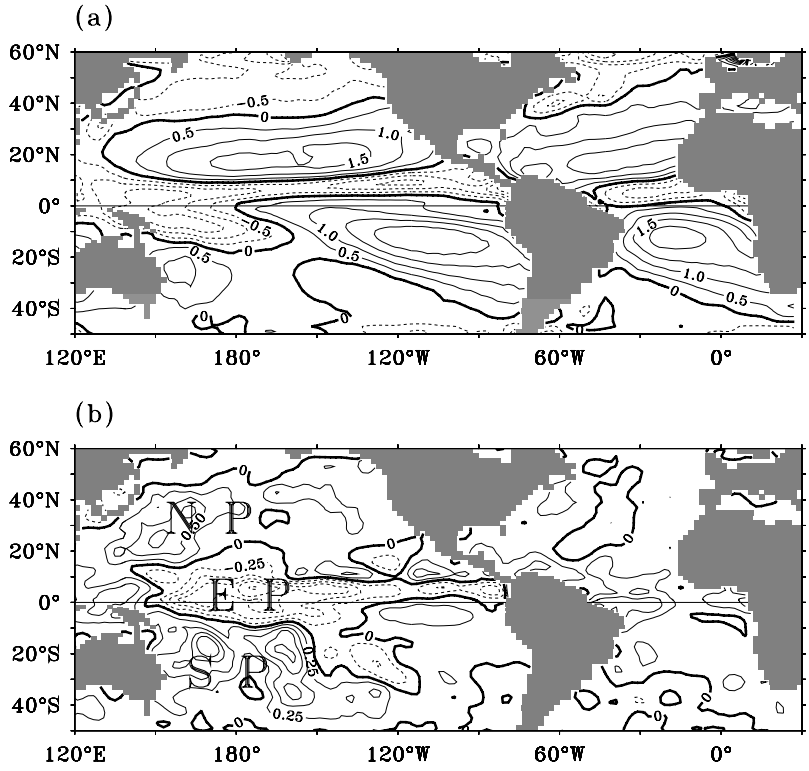

Figure 1. (a) Average EmP between 1988 and 2000. The contour interval is 0.5 m yr^{-1}. (b) The difference between the EmP average in Figure 1a and 1988 EmP. The contour interval is 0.25 m yr^{-1}. Negative values are shown as dashed contours.

and PTB were designed to explore the overall impact of EmP on ocean salinity, circulation, and temperature. As shown in Figure 1b, the EmP anomalies were of opposite signs between subtropical and tropical Pacific. Therefore we designed three additional experiments to separate their individual roles in affecting the Pacific Ocean: Experiments NP, EP, and SP (Table 1) were forced by monthly EmP between 1988 and 2000 in region NP, EP, and SP (Figure 1b), respectively, while monthly EmP of 1988 was specified in other regions as in CTR. Since surface flux boundary condition was applied for model SST in our experiments, it is important to test the sensitivity of ocean temperature anomalies to the surface boundary condition. Therefore additional control (CRS1-3, Table 1) and perturbation (PRS1-3) experiments were designed with the same forcings as in CTR and PTB except for an additional SST restoration with timescales τ_2 of 60, 30, and 10 days, respectively,

$$dT/dt = Q_{Model} + (SST - T)/\tau_2. \quad (4)$$

Table 1. Experiments With the MIT Ocean General Circulation Model[a]

Experiment	EmP		SST Boundary Condition
	Time Period	Region	
CTR	1988	global	heat flux
PTB	1988–2000	global	heat flux
NP	1988–2000	North Pacific positive EmP	heat flux
EP	1988–2000	equatorial Pacific negative EmP	heat flux
SP	1988–2000	South Pacific positive EmP	heat flux
CRS1	1988	global	heat flux and damping of 8, 17, and 50 Wm^{-2} K^{-1}.
CRS2			
CRS3			
PRS1	1988–2000	global	heat flux and damping of 8, 17, and 50 Wm^{-2} K^{-1}.
PRS2			
PRS3			

[a]Boundaries of regions NP, EP, and SP are shown in Figure 1b.

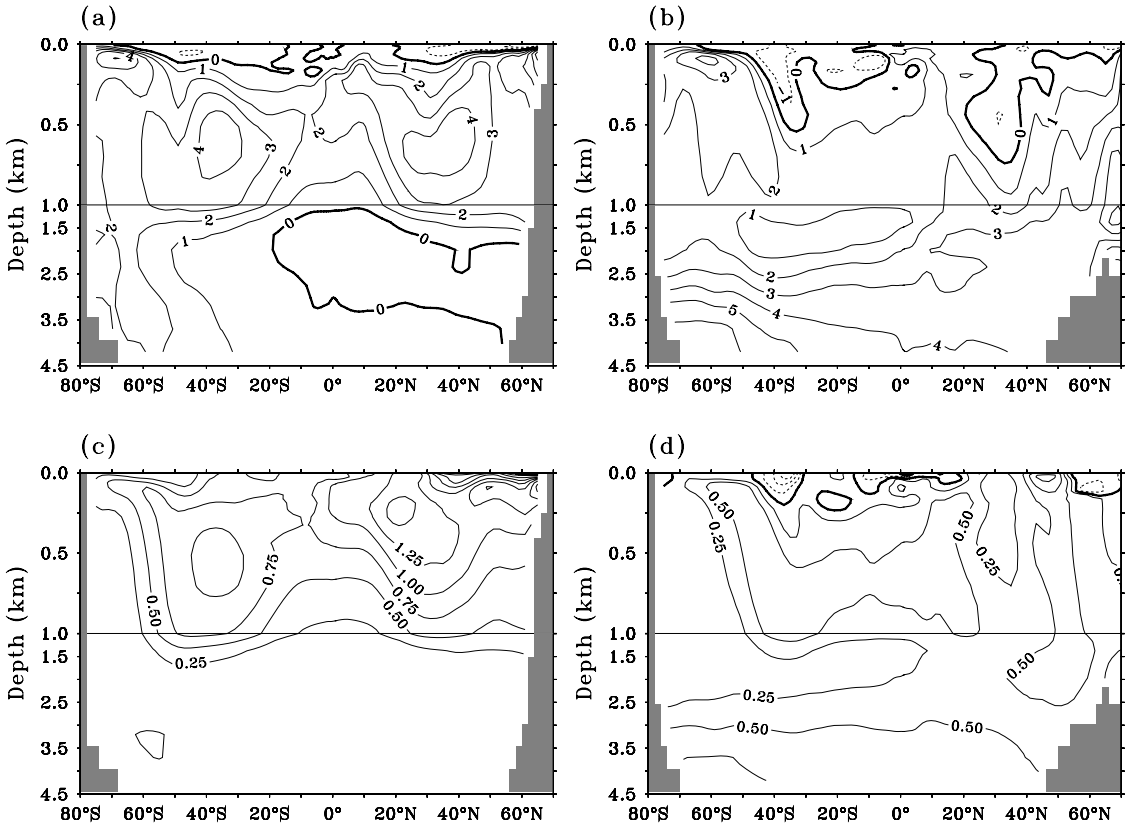

Figure 2. Difference between simulated and observed (Levitus) climatologies of (a) temperature in the Pacific, (b) temperature in the Atlantic, (c) salinity in the Pacific, and (d) salinity in the Atlantic. The contour intervals are 1°C in Figures 2a and 2b, and 0.25 psu in Figures 2c and 2d.

These restoration timescales are equivalent to 8 [*Yang et al.*, 1999], 17, and 50 Wm^{-2} K^{-1}, respectively, in heat flux damping. The temperature of water precipitating into the ocean was assumed to be the same as the model SST as that of *Yang et al.* [1999]. All experiments were integrated for 13 years from 1988 to 2000. The difference relative to CTR (or CRS1-3) is defined as an anomaly.

[12] The OGCM simulated observed temperature and salinity climatology of the Pacific and Atlantic oceans reasonably well (Figure 2). The error between simulated and observed temperature was about 3°–4°C between 300 and 1000 m in the Pacific, and below 3000 m in the Atlantic (Figures 2a and 2b). The salinity error was larger in the Pacific (1 psu) than in the Atlantic (0.5 psu, Figures 2c and 2d). These errors are comparable to errors in other OGCM simulations [*Jiang et al.*, 1999], which is largely due to strong vertical diffusivity and is a general problem in OGCMs.

4. Average Responses During 1988–2000

4.1. Responses Near the Ocean Surface

[13] Figure 3a shows average salinity anomalies between PTB and CTR and average currents in PTB from the ocean surface to 50 m during 1989 and 2000 in the Pacific and Atlantic oceans. Salinity decreased 0.2–0.5 psu in the equatorial and tropical Pacific between 10°S and 20°N, increased 0.2–0.5 psu in the subtropical North Pacific between 20°N and 40°N, and increased 0.5–1 psu in the subtropical South Pacific between 40°S and 20°S. In the Atlantic, surface salinity increased approximately 0.2 psu between 20°S and 20°N and decreased 0.1–0.2 psu in the central subtropical North and South Atlantic. Analyses (not shown) indicated that the spatial patterns of these anomalies during the 1988 to 2000 period are representative of both earlier (before 1995) and later (after 1995) years, although their strengths were larger in the later years.

[14] Distributions of these salinity anomalies were generally consistent with the EmP anomalies shown in Figure 1b. This suggests that salinity anomalies resulted directly from local anomalous EmP by changes in vertical mixing, although they were transported to other regions by average ocean currents. For example, the center of negative EmP anomaly was located at approximately 5°N in the tropical Pacific, but the center of negative salinity anomaly was located at approximately 15°N, which was largely due to strong northward transport of fresher water by the average Ekman flow (Figure 3a). The saltier water in the tropical Atlantic due to anomalous EmP was transported northward by the Guiana Current and the Gulf Stream.

[15] In contrast, the distribution of temperature anomalies (Figure 3b) was different from the EmP and salinity anomalies. In the Pacific Ocean, the average temperature between the ocean surface and 50 m decreased approximately 0.2°C between 20°S and 15°N, 0.2°C in the northwest North Pacific north of 30°N, and 0.5°C in the South Pacific east of Australia. The average temperature increased approximately 0.5°C in a southwest-to-northeast oriented

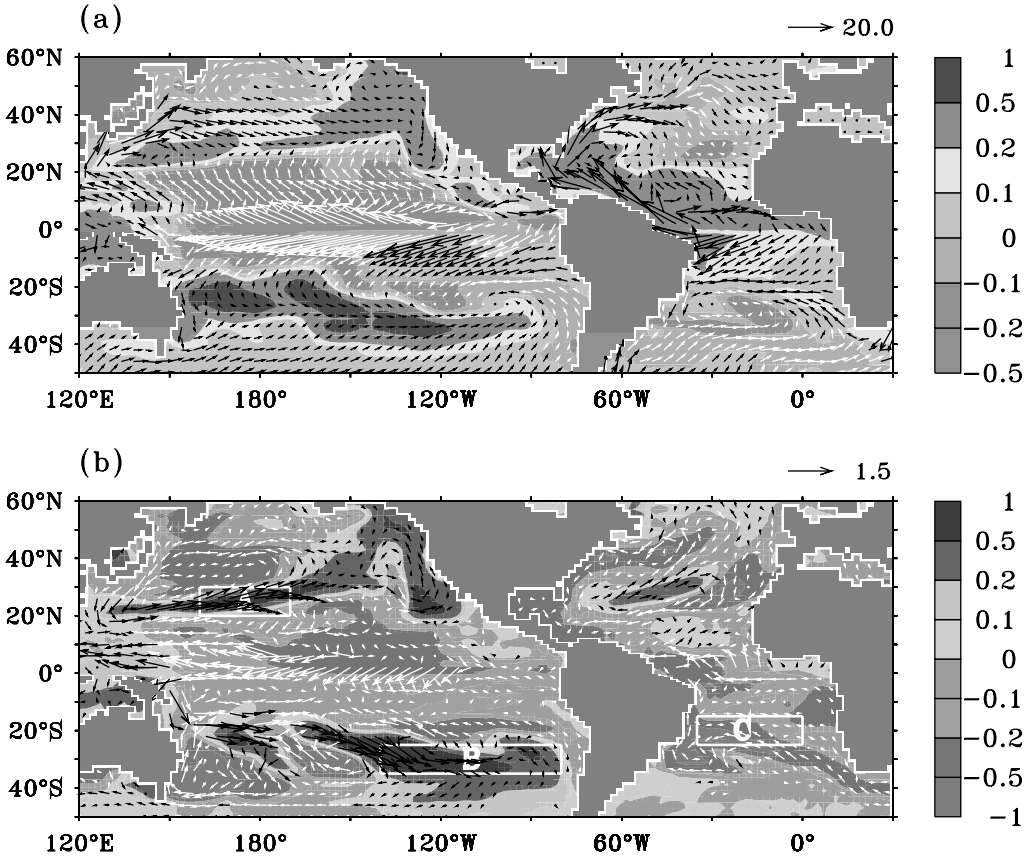

Figure 3. (a) Averaged (1988 to 2000) near-surface (0 to 50 m) salinity anomaly (shaded, °C) between PTB and CTR, and average currents (vector, 20 cm s^{-1}) in PTB. (b) Average near-surface (0 to 50 m) temperature (shaded) and current (vector, 1.5 cm s^{-1}) anomalies between PTB and CTR. Vector colors are changed to increase contrast with background shading. Vectors are shown on 4° longitude and 4° latitude grids. Regions A, B, and C are shown as rectangular boxes. See color version of this figure at back of this issue.

region from 130°E–20°N to 130°W–50°N, and 0.5°–1.0°C in the South Pacific between 20°S and 40°S. In the Atlantic Ocean, the average temperature decreased 0.2°–0.5°C between 40°S and 40°N, except in a small region near 45°W–30°N where it increased approximately 0.2°C.

[16] These temperature anomalies were largely associated with anomalous ocean currents (Figure 3b), especially in the Pacific Ocean. The cooling in the western subtropics of the North and South Pacific resulted from a reduced heat transport due to a weakened Kuroshio and a weakened East Australia Current (EAC). The warming in the eastern subtropics of the North and South Pacific resulted from reduced cooling due to weakened equatorward interior flows. The cooling in the tropical Pacific was associated with a larger cold advection due to a stronger South Equatorial Current (SEC). In the Atlantic Ocean, the cooling along the east coast of North America and along the Gulf Stream extension was associated with a weakening of the Gulf Stream (Figure 3b). The warming in the central North Atlantic was clearly due to anomalous northward currents or weakened subtropical interior flows. In contrast, the cooling in the South Atlantic was associated with stronger equatorward interior flows. The cooling in the tropical Atlantic was associated with a stronger SEC.

[17] The combination of weakened western boundary currents and interior flows indicates that the subtropical gyres were spun down; this effect was relatively stronger in the Pacific than in the North Atlantic. The spindown of the subtropical gyres in the Pacific was associated with distributions of positive EmP anomalies in the subtropics and negative EmP anomalies in the tropics. This was consistent with the Stommel-Goldsbrough circulation theory [*Goldsbrough*, 1933; *Stommel*, 1984; *Huang*, 1993] that the subtropical gyre spins up (down) when precipitation (evaporation) increases. Goldsbrough originally proposed that the downward velocity due to falling raindroplets could result in a large-scale circulation, which would be true no matter whether the oceans were salty or fresh. This may be explained simply by potential vorticity conservation: c = f/h where f is the Coriolis parameter and h is water column depth. If a water column is squeezed (reduced h) owing to falling raindroplets, it has to move southward to conserve potential vorticity (to reduce f) that causes the subtropical gyre to spin up. In contrast, the subtropical gyre spins down due to evaporation. In the oceans with salty water, the spindown of the subtropical gyres in the Pacific may also be associated with the higher density or heavier water within the gyre due to positive EmP anomalies (more evaporation

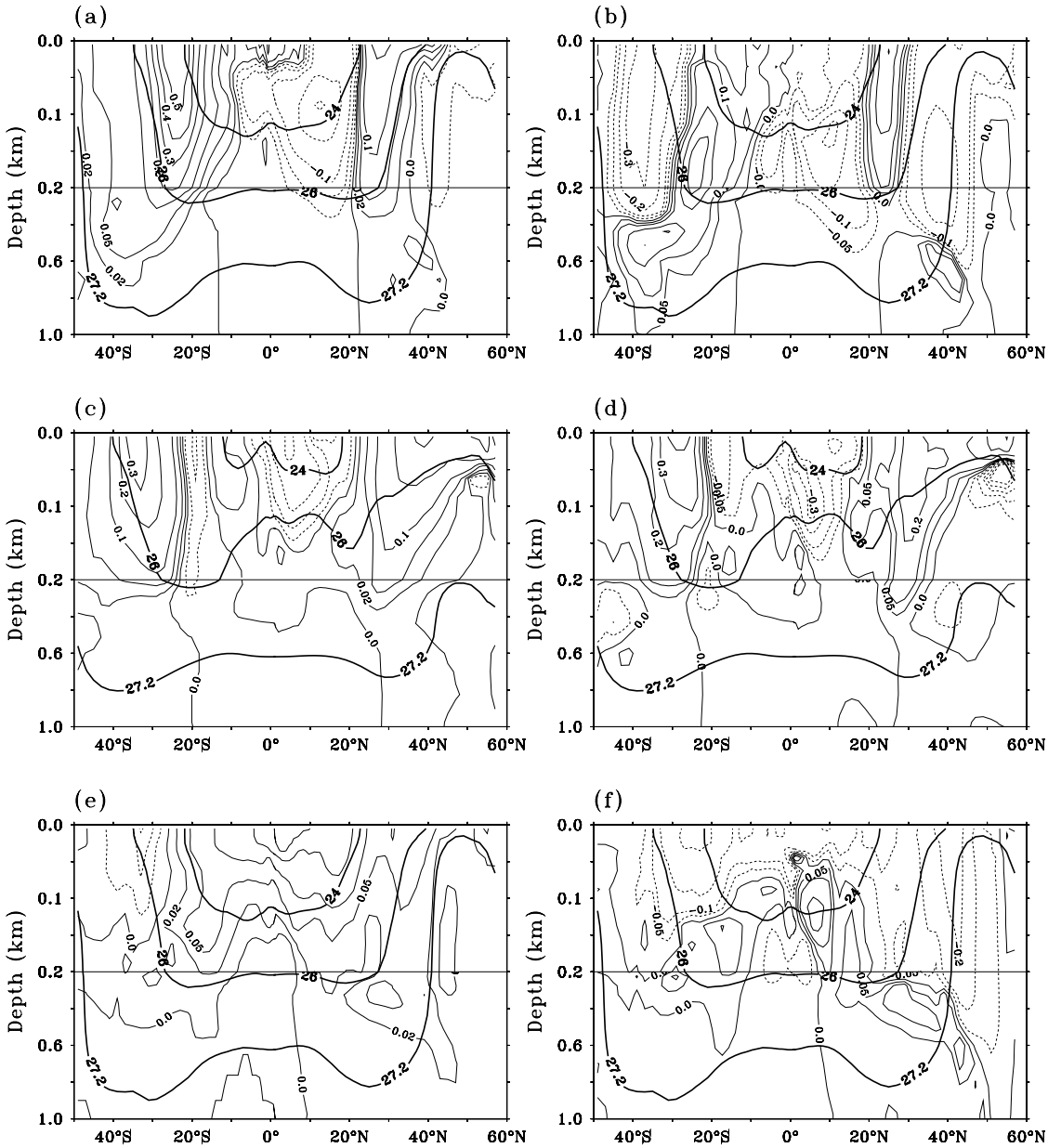

Figure 4. Time-averaged (1988 to 2000) and zonally averaged anomalies of (a) salinity in the western Pacific between 120°E and 160°W, (d) salinity in the eastern Pacific between 160°W and 70°W, and (e) salinity in the Atlantic. Figures 4b, 4d, and 4f are the same as Figures 4a, 4c, and 4e, except for temperature. The contours are 0, ±0.02, ±0.05, ±0.1, ±0.2, ±0.3, ±0.4, and ±0.5 psu in Figures 4a, 4c, and 4e; and the contours are 0, ±0.05, ±0.1, ±0.2, ±0.3, and ±0.4°C in Figures 4b, 4d, and 4f. Zonally averaged and time-averaged simulated density contours are shown as heavy solid contours of 24, 26, and 27.2 Kg m^{-3}.

or less precipitation), since the wind forcing was specified to its monthly climatology. Another possibility resulting in the spindown of the subtropical gyre is the stronger vertical mixing by saltier surface water due to positive EmP anomalies, which can more effectively transport momentum fluxes from the surface to the deeper layer, and therefore the subtropical gyres near the surface were spun down. The effects of changes in density and vertical mixing due to anomalous EmP on the subtropical gyre circulation may explain why the subtropical gyre circulation can also be affected by changes in tropical precipitation (see section 6), since the fresher water is transported to the subtropical ocean. Similarly, the saltier water in the North Atlantic Ocean was transported to higher latitudes by the Guiana Current and the Gulf Stream, which increased the salinity (Figure 3a) and density and spun down the subtropical gyre. In the South Atlantic, however, the subtropical gyre was spun up slightly due to a decrease of salinity resulting from anomalous EmP.

[18] As shown in Figure 3b, temperature changes in the Pacific Ocean were largely associated with anomalous heat transports due to changes in currents. Heat budget analyses

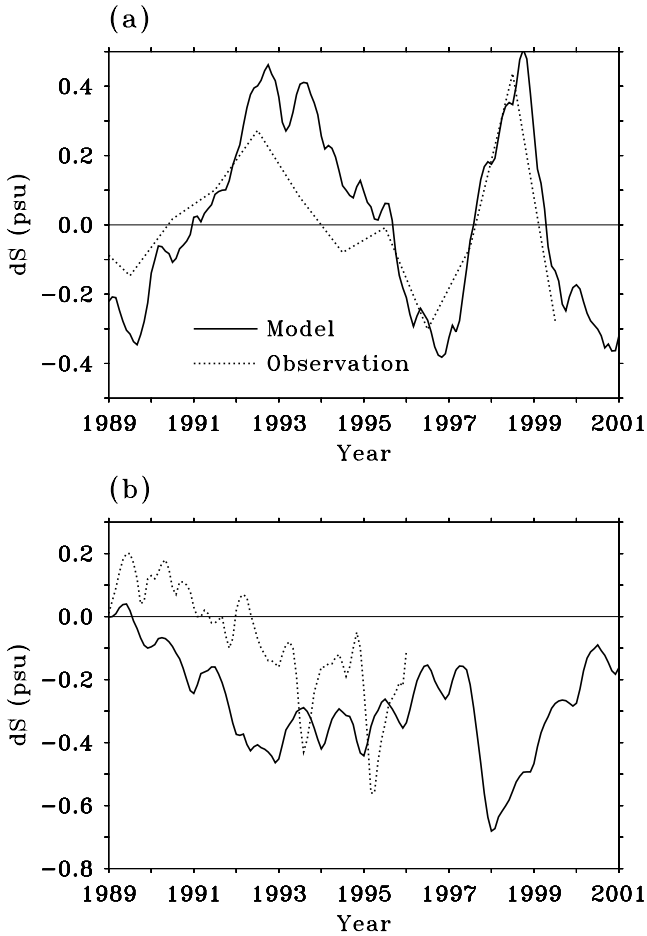

Figure 5. Simulated and observed anomalous sea surface salinity (psu) averaged within (a) 125°E–140°E and 0°–10°N, and (b) 170°W–120°W and 0°–10°N. Observed annual salinity in Figure 5a was obtained from www.nodc.noaa.gov, and observed monthly salinity in Figure 5b was obtained from *Delcroix et al.* [2000b].

(see more details in section 5.2) also confirmed the important role of advective heat transport in temperature changes. However, the analyses indicated that vertical mixing played a dominant role in temperature changes in the Atlantic Ocean. The reason for the major roles of advection and vertical mixing in the Pacific and Atlantic oceans, respectively, may result from the differences in anomalous EmP. The positive anomalous EmP in the Atlantic was located in the tropics, and its magnitude (0.5 m yr^{-1}) and areal extent were relatively small. In contrast, the positive anomalous EmP in the Pacific was located in the subtropics and its magnitude (0.75 m yr^{-1}) and areal extent were large. Therefore the spindown of the subtropical gyres in the Pacific was more severe than that in the Atlantic. As a result, temperature changes due to heat advection changes dominated over those due to vertical mixing changes in the Pacific, but it was the opposite case in the Atlantic.

4.2. Zonally Averaged Responses

[19] To assess the effects of anomalous EmP on the subsurface oceans, zonally averaged salinity and temperature anomalies were analyzed. We separated the zonal averages in the western (120°E–160°W) and eastern (160°W–70°W) Pacific Ocean due to asymmetric temperature anomalies in longitudinal direction (Figure 3b). In the western Pacific, salinity (Figure 4a) decreased 0.1–0.3 psu between 10°S and 20°N from the ocean surface to 200 m, and increased 0.1–0.2 psu between 20°N and 40°N and 0.1–0.4 psu south 10°S above 200 m. In the eastern Pacific, salinity changes (Figure 4c) were similar to those in the western Pacific. In the Atlantic Ocean (Figure 4e), salinity increased 0.1–0.3 psu between 20°S and 30°N from the ocean surface to 100 m.

[20] Similar to the salinity anomalies, the structures of temperature anomalies were vertically oriented in the Pacific Ocean. In the western Pacific (Figure 4b), temperatures decreased 0.1°–0.3°C between 10°S and 20°N above 500 m, 0.2°C between 30°N and 50°N above 600 m, and 0.1°–0.3°C south of 25°S above 400 m. Temperatures increased 0.1°–0.2°C between 20°N and 30°N above 200 m, 0.1°–0.2°C between 25°S and 15°S above 400 m, and 0.2°C near 35°S between 400 and 800 m. In the eastern Pacific (Figure 4d), the cooling in the lower latitudes was shallower than that in the west, and temperature increased approximately 0.2°–0.3°C in the higher latitudes above 200 m except near 50°N and 50 m where a cooling was found. In the Atlantic Ocean (Figure 4f), temperature generally decreased near the surface (0.1°–0.3°C) from 40°S to 50°N, but increased in the subsurface (0.1°–0.2°C) ocean, especially near the equator. Density anomalies (not shown) in the Pacific and Atlantic oceans were largely associated with salinity anomalies, which were directly forced by anomalous EmP from the ocean surface to 200 m. The density changes due to changed temperature and salinity canceled each other in the subsurface oceans below 200 m, which is similar to the spiciness hypothesis proposed by *Schneider* [2000].

5. Interannual Response During 1988–2000

5.1. A Comparison of Simulated and Observed Surface Salinity

[21] In the western equatorial Pacific (125°E–140°E and 0°–10°N), the simulated SSS from early 1989 to late 1999 agreed very well with observations from the NOAA Oceanographic Data Center (NODC; www.nodc.noaa.gov) in both magnitude and phase (Figure 5a). This suggests that SSS changes were largely due to EmP changes in the western Pacific Warm Pool. In the central equatorial Pacific (170°W–120°W and 0°–10°N); however, the discrepancy between the simulated and observed SSS from *Delcroix et al.* [2000b] was relatively large during 1989 and 1996 (Figure 5b), although the overall decreasing trend in SSS was simulated reasonably well. This larger discrepancy in the central equatorial Pacific may indicate that interannual changes in wind stress and heat flux which were not applied in our experiments had a strong influence on SSS by changes in the SEC. Uncertainties in observed SSS may also be large in the central Pacific owing to sparse data and uncertainties in EmP estimates are not known.

[22] Overall, in the equatorial Pacific Ocean, the simulated anomalous salinity (Figure 6b) was largely associated with anomalous EmP (Figure 6a). Furthermore, the simulated salinity anomalies were consistent with observations

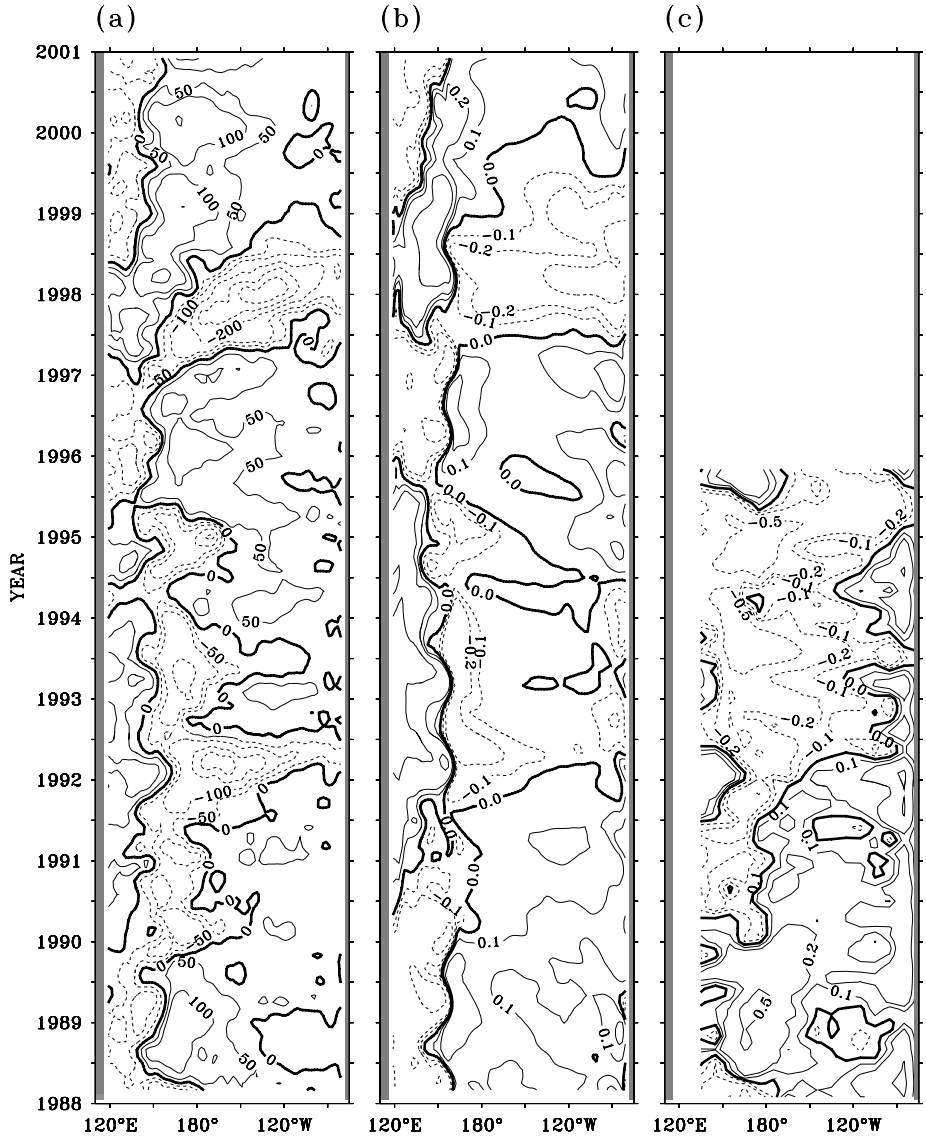

Figure 6. (a) Observed EmP anomaly, (b) simulated SSS anomaly, and (c) observed SSS anomaly averaged between 2°S and 2°N and between 0 and 50 m. The contour intervals are 50 cm yr^{-1} in Figure 6a; and contours are 0, ±0.1, ±0.2, and ±0.5 psu in Figures 6b and 6c. Observed SSS was obtained from *Delcroix et al.* [2000b].

by *Delcroix et al.* [2000b] in Figure 6c, although the discrepancy between the simulated and observed SSS anomalies was also notable in the eastern equatorial Pacific after 1995. In addition, the east-west migration of the SSS front in the western Pacific in the simulation was not as strong as in the observations by *Matsuukra and Iizuka* [2000] during the 1991–1992 El Niño event. The reason might be a lack of strong westerly wind bursts and associated eastward anomaly of the SEC in our simulation, as indicated in the observations by *Delcroix et al.* [2000a], *Henin et al.* [1998], *Vialard and Delecluse* [1998b], and *Frankignoul et al.* [1996]. At middle and high latitudes, comparisons between the simulated and observed SSS were not possible owing to a lack of observational data. In the Atlantic Ocean, the comparison between simulated and observed SSS from NODC was less consistent, largely owing to discontinuities of observed data even in regions where relatively more data were available, such as near 10°N–45°W and near 40°N–45°W.

[23] While the simulation of interannual salinity variability in the equatorial Pacific Ocean was largely consistent with observations, we should not expect observed and simulated temperatures to agree with each other [*Huang and Mehta*, 2004]. The reason is that the observed temperature variability is due to combined effects of wind stress, surface heat flux, and EmP, whereas the temperature variability in our simulation was influenced by EmP variability only.

5.2. Interannual Variability

[24] To analyze interannual responses of the Pacific and Atlantic Oceans to interannually varying EmP, we selected three regions, two in the Pacific (region-A: 20°N–30°N and 160°E–170°W, and region-B: 35°S–25°S and 140°W–

80°W) and one in the Atlantic (region-C: 25°S–15°S and 40°W–0°) as shown in Figure 3b. The selection was based on the relatively stronger temperature anomalies in these regions. The interannual variability of salinity was small in region-A in the North Pacific (Figure 7a), and seasonal variations with a typical amplitude of 0.2 psu can be identified clearly. The temperature in this region, however, exhibited a pronounced interannual variability with approximately 0.5°C amplitude, which increased from 1989 to 1993 and decreased from 1997 to 2000. In region-B of the South Pacific (Figure 7b), salinity decreased slightly from 1989 to 1992 and increased approximately 0.7 psu by 2000; and temperature in this region increased approximately 1°C from 1989 to 2000. The indication is that the temperature anomaly may not result directly from local salinity change, since the change in salinity lagged the change in temperature. In region-C of the South Atlantic (Figure 7c), salinity increased very slightly, with a clear seasonal variability, and temperature decreased 0.9°C monotonically from 1990 to 2000.

[25] Overall, there were no clear relationships between the local variabilities of salinity and temperature when effects from changes in surface heat flux and wind stress were not considered. This suggests that the mechanisms resulting in salinity and temperature variabilities due to anomalous EmP forcing were different: The salinity anomalies were driven directly by anomalous EmP and transported by average ocean circulation (refer to Figure 3a); the temperature anomalies, however, were associated largely with anomalous ocean circulations in the Pacific (refer to Figure 3b) but with changes in vertical mixing in the Atlantic. In addition, the period of oceanic response may be longer than 20 years in all regions, although it cannot be proven in this study due to the relatively short simulation time. This is different from the tropical Pacific and the Indo-Pacific Warm Pool [*Huang and Mehta*, 2004] where the ocean responded to surface EmP forcing at timescales of 3–5 years, as well as at the decadal timescale.

[26] To quantify the relative contributions of ocean circulations and mesoscale eddy mixing, we diagnosed heat budgets as done by *Huang and Mehta* [2004]. The anomalous total (local) tendencies of temperature were decomposed into anomalous ocean advection and vertical mixing,

$$T_t = T_{adv} + T_{mix}, \tag{5}$$

where T_t is anomalous local temperature tendency,

$$T_{adv} \equiv -u\partial_x T - v\partial_y T - w\partial_z T \tag{6}$$

is anomalous temperature advections, and

$$T_{mix} = T_{zz} + T_{KPP} + Q_{Model} \tag{7}$$

is anomalous vertical mixing of temperature, which includes vertical diffusion, non-local KPP mixing, and surface source terms. The term for horizontal mixing was small and ignored in our analyses. The combination of these terms was based on the similarity of their dynamic properties and the fact that they largely canceled each other. The source term was treated as an upper surface boundary condition. Temperature anomalies due to various terms can be integrated as

$$\Delta T_{total} = \sum_{1988}^{t} T_t \cdot \delta t, \tag{8}$$

$$\Delta T_{adv} = \sum_{1988}^{t} T_{adv} \cdot \delta t, \tag{9}$$

$$\Delta T_{mix} = \sum_{1988}^{t} T_{mix} \cdot \delta t, \tag{10}$$

where tendency terms T_t, T_{adv}, and T_{mix} were calculated at each time step (3 hours) during the experiments, and their monthly averages were output for analyses. Here δt (1 month) is the time interval of model outputs. By comparing the signs and evolutions of total anomalies with those due to ocean advection and vertical mixing, one can determine dominant processes causing interannual variability.

[27] The heat budget analysis indicated that the temperature anomaly was largely due to changes in ocean heat advection in region-B (Figure 8b) in the South Pacific, which dominated those due to changes in vertical mixing. The 1.5°C temperature anomaly due to anomalous heat advection was much larger than that due to anomalous vertical mixing (−0.2°C). The temperature anomaly resulted from both anomalous heat advection and vertical mixing in region-A (Figure 8a). The total temperature anomaly (0.5°C) followed the temperature anomaly due to anomalous heat advection before 1995, with little influence from vertical mixing. The total temperature anomaly, however, was maintained largely due to a gradual enhancement of vertical mixing (1°C) after 1995. In region-C in the South Atlantic (Figure 8c), changes in vertical mixing played a dominant role in the total temperature anomaly. Temperature decreased approximately 2°C due to anomalous vertical mixing, but increased only approximately 1.2°C owing to anomalous heat advection from 1989 to 2000. Their combined effect resulted in an approximate 0.8°C decrease of the total temperature anomaly.

6. Effects of Regional EmP Anomalies and SST Restoring

[28] As shown in section 4.1 (Figure 3b), the changes in ocean temperature near the ocean surface resulted from anomalous currents in the Pacific Ocean; the changes in ocean circulations, in turn, resulted from the spindown of the subtropical gyres; and the spindown of these gyres was forced by anomalous EmP (Figure 1b) which was positive (more evaporation or less precipitation) in the subtropical North and South Pacific and negative (more precipitation or less evaporation) in the equatorial Pacific. What was the individual contribution of these positive and negative EmP anomalies to the changes in temperature and circulations in the Pacific? The results from experiments NP, EP, and SP answer this question.

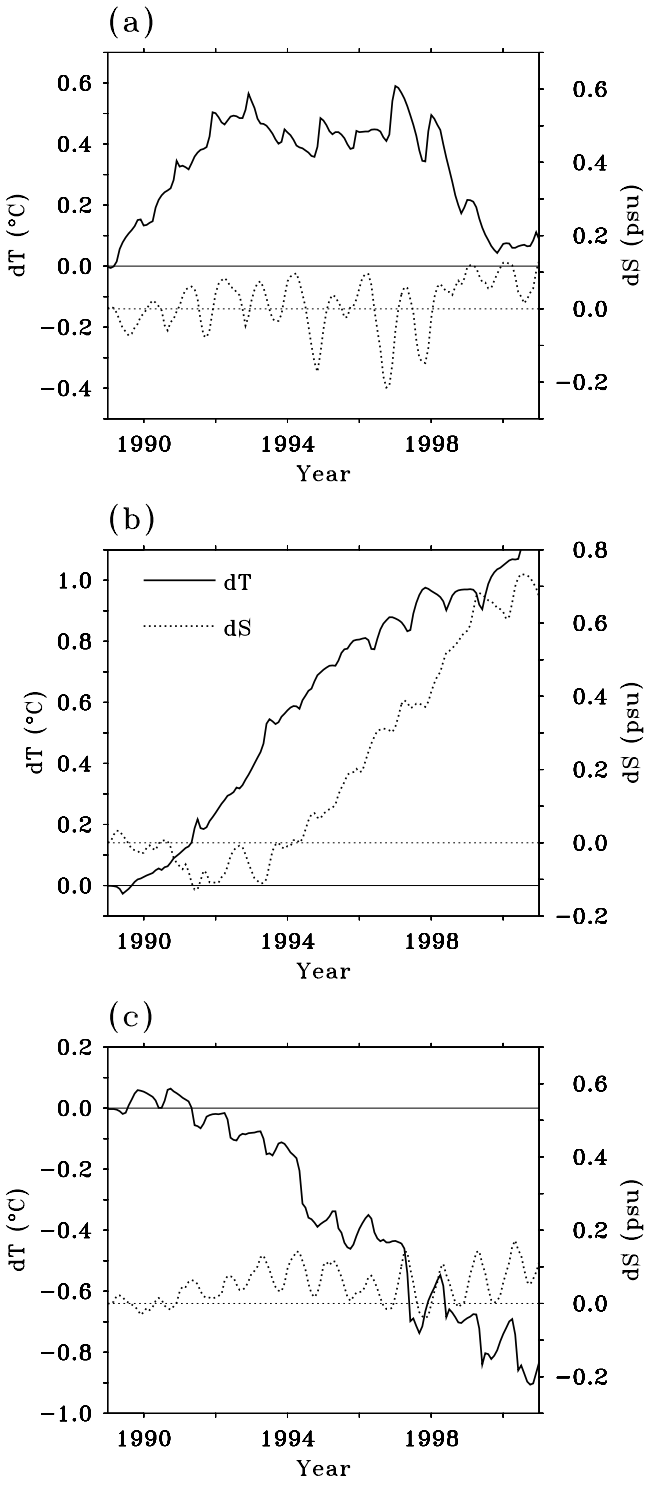

Figure 7. Anomalous temperature (left coordinate, °C) and salinity (right coordinate, psu) from 1989 to 2000 in (a) region-A, (b) region-B, and (c) region-C averaged between 0 and 50 m. The locations of these regions are shown in Figure 3b and explained in text.

[29] When forced with positive anomalous EmP in the subtropical North (Figure 9a) and South (Figure 9c) Pacific in NP and SP, salinity anomalies between the ocean surface and 50 m were largely confined within the subtropical oceans owing to average, convergent Ekman flows. When forced with negative EmP in the equatorial Pacific (Figure 9b) in EP, surface salinity anomaly dispersed toward the west and higher latitudes to 20°S and 30°N. It is important to note that the salinity anomalies due to com-

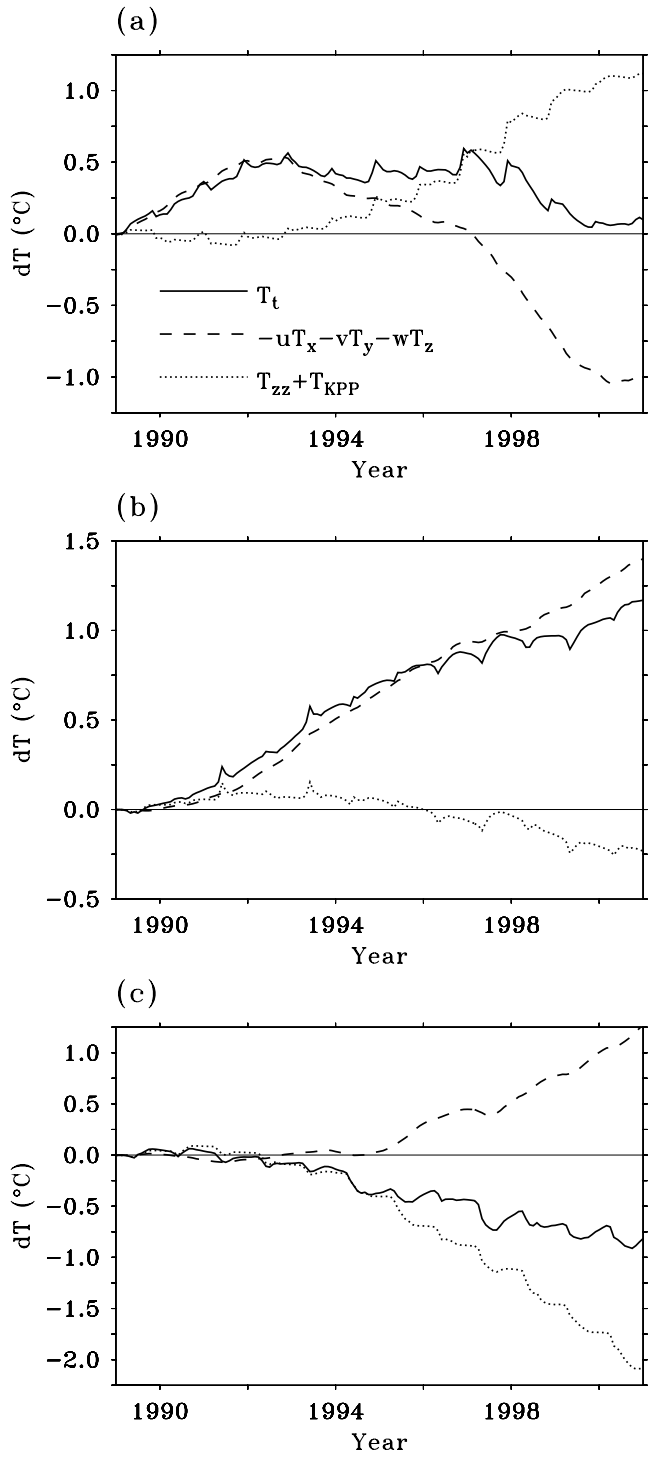

Figure 8. Accumulated temperature changes (°C) due to local tendency, advection, and vertical mixing in (a) region-A, (b) region-B, and (c) region-C averaged between 0 and 50 m. The locations of these regions are shown in Figure 3b and explained in text.

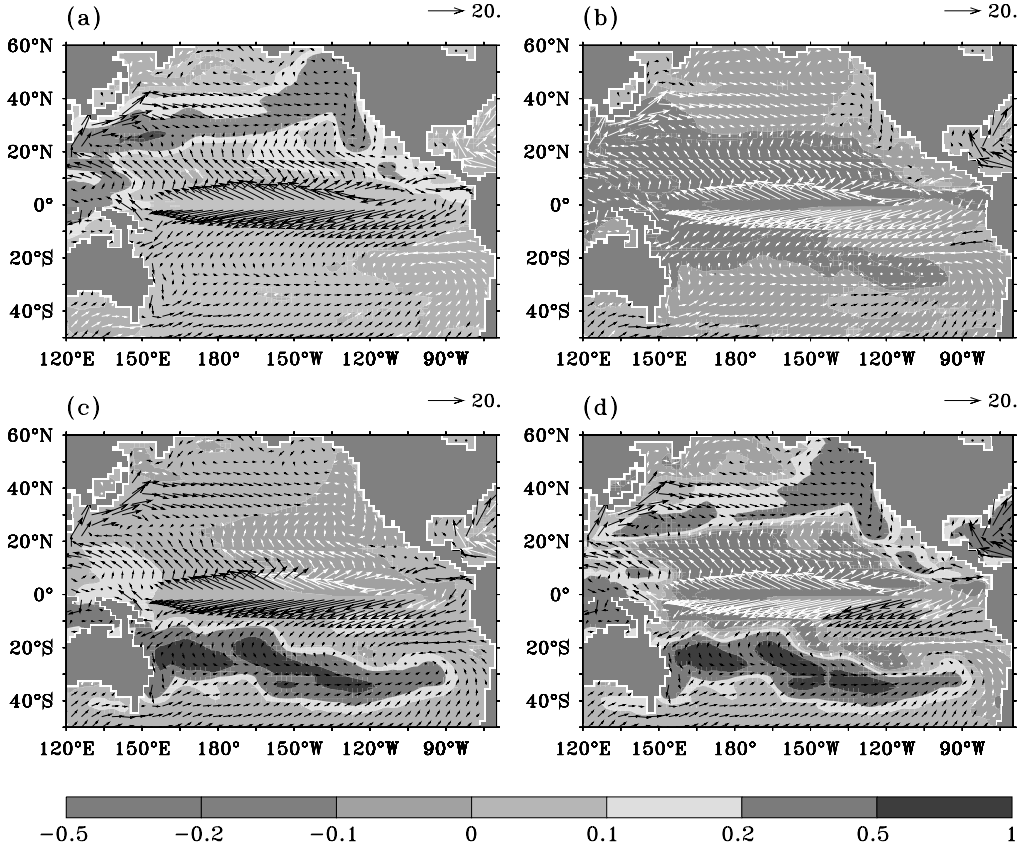

Figure 9. Averaged (1988 to 2000) near-surface (0 to 50 m) salinity anomalies (shaded, psu) and average currents (vector, 20 cm s^{-1}) in (a) NP, (b) EP, (c) SP, and (d) PTB. Vector colors are changed to increase contrast with background shading. Vectors are shown on a 4° longitude × 4° latitude grid. See color version of this figure at back of this issue.

bined EmP forcing (Figure 9d, same as Figure 3a) are almost a linear summation of those in NP, EP, and SP due to each individual EmP forcing.

[30] When salinity, and therefore density, increased in the subtropical Pacific in NP and SP, the subtropical gyres spun down (Figures 10a and 10c). The Kuroshio, EAC, and interior flows became weaker. The change in these circulations resulted in a cooling in the west and a warming in the east due to anomalous heat advection by anomalous ocean currents. The cooling in the western subtropics reached the western boundary, propagated equatorward along the western boundary as coastal Kelvin waves, and propagated eastward along the equator as equatorial Kelvin waves (see *Huang et al.* [2005] for more details). As a result, a cooling appeared in the tropical Pacific and the SEC became stronger. When salinity and density decreased between 20°S and 30°N in EP, the vertical mixing became weaker. This contributed largely to the surface warming (Figure 10b) in the tropical and subtropical Pacific. The warming resulting from weaker vertical mixing due to negative anomalous EmP in EP was similar, in an opposite sense, to the cooling resulting from stronger vertical mixing due to positive EmP in the Atlantic Ocean in PTB shown in Figure 3b. The spinup of the subtropical gyres due to decreased salinity and density further intensified the warming in the western North Pacific and in the central South Pacific near 30°S–130°W. Similar to the salinity anomalies, the temperature anomalies (Figure 10d, same as Figure 3b) due to combined EmP forcing in PTB were almost a linear summation of those in NP, EP, and SP. The resultant ocean circulation and temperature anomalies, however, were dominantly driven by anomalous EmP in the subtropics.

[31] The oceanic response to anomalous EmP was also found to be linear in the subsurface layers. When forced by positive anomalous EmP in the North Pacific in NP (Figure 11a), a positive temperature anomaly developed near 20°N above 500 m and a negative temperature anomaly developed near 40°N above 600 m. These temperature anomalies were directly associated with the spindown of the subtropical gyre in the North Pacific. A cooling developed in the tropics above 100 m, which was associated with the propagation of coastal Kelvin waves from the subtropics. The results in SP (Figure 11c) were very similar to those in NP except that the cooling propagating to the tropics became stronger due to larger anomalous EmP. When forced by negative anomalous EmP in the tropical Pacific in EP (Figure 11b), temperature increased near the surface and decreased in the subsurface ocean, which was opposite to the temperature anomalies in the Atlantic shown in Figure 4f due to positive anomalous EmP. The temperature

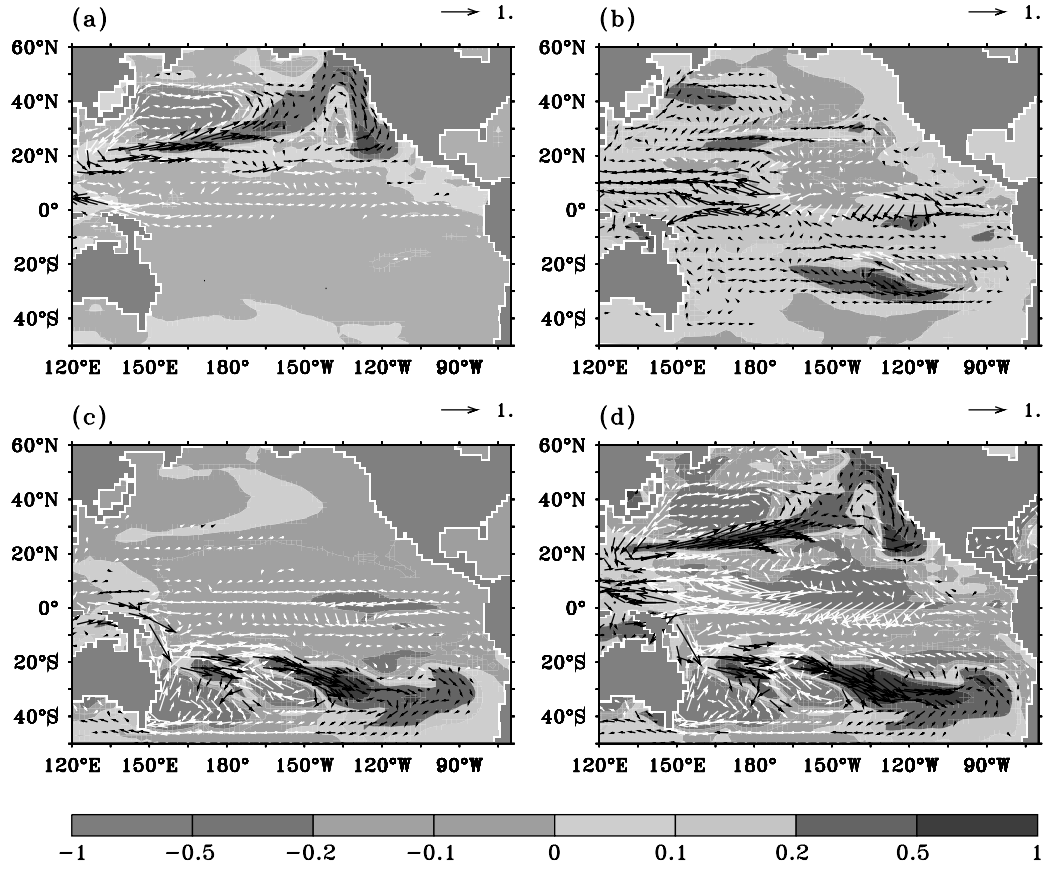

Figure 10. Averaged (1988 to 2000) near-surface (0 to 50 m) temperature (shaded, psu) and current (vector, 1 cm s^{-1}) anomalies in (a) NP, (b) EP, (c) SP, and (d) PTB. Vector colors are changed to increase contrast with background shading. Vectors are shown on a 4° longitude × 4° latitude grid. See color version of this figure at back of this issue.

anomalies linearly added from NP, EP, and SP were almost the same as those in PTB shown in Figure 12a.

[32] Finally, we note that all experiments up to this point were conducted using the surface flux boundary condition on the model SST. It is important, however, to clarify whether the oceanic responses in our simulation were critically dependent on the surface boundary condition, since temperature anomalies can be damped away by changes in surface heat flux. Experiments CRS1 and PRS1 (Table 1), using an additional 8 Wm^{-2} K^{-1} damping (comparable to the damping used by *Yang et al.* [1999]) indicated that the temperature anomalies between PRS1 and CRS1 in the Pacific (Figure 12b) were very similar to those without the damping (Figure 12a) except for a slight weakening near the surface. This indicated that the temperature anomalies below the surface in the Pacific due to anomalous EmP were not very sensitive to the surface boundary condition. The reasons were that these temperature anomalies were largely associated with changes in ocean circulations which, in turn, were associated with density changes due to anomalous EmP as described in section 4. In the Atlantic Ocean (Figure 13b), however, the cooling near the surface was largely weakened by surface damping when it was compared with that without the surface damping (Figure 13a), although the warming in the subsurface was less affected. The reason was that the surface cooling in the Atlantic was associated with anomalous vertical mixing (see Figure 8c) which was critically dependent on the surface boundary condition.

[33] When the surface damping coefficient was further increased to 17 Wm^{-2} K^{-1} in experiments PRS2 and CRS2 (Table 1), the temperature anomalies in the Pacific below 50 m (Figure 12c) did not change very much if they were compared with those in Figure 12b, although SST anomalies were largely damped. In the Atlantic Ocean (Figure 13c), changes in temperature anomalies were also very small below 50 m if they were compared with those in Figure 13b. We also conducted another set of experiments PRS3 and CRS3 with the surface damping coefficient 50 Wm^{-2} K^{-1}; the same coefficient was used during the initial model spinup. The temperature anomalies between PRS3 and CRS3 in the subsurface ocean were almost the same as those between PRS2 and CRS2 in both the Pacific (Figure 12d) and the Atlantic (Figure 13d). These experiments indicated that anomalous EmP can force the subsurface ocean temperatures to change even when a fairly strong atmospheric damping to SST was applied.

7. Summary

[34] We studied the responses of the upper Pacific and Atlantic Oceans to satellite-based EmP estimates from 1988 to 2000 using the MIT OGCM. Relative to 1988, EmP anomalies were positive (more evaporation or less precip-

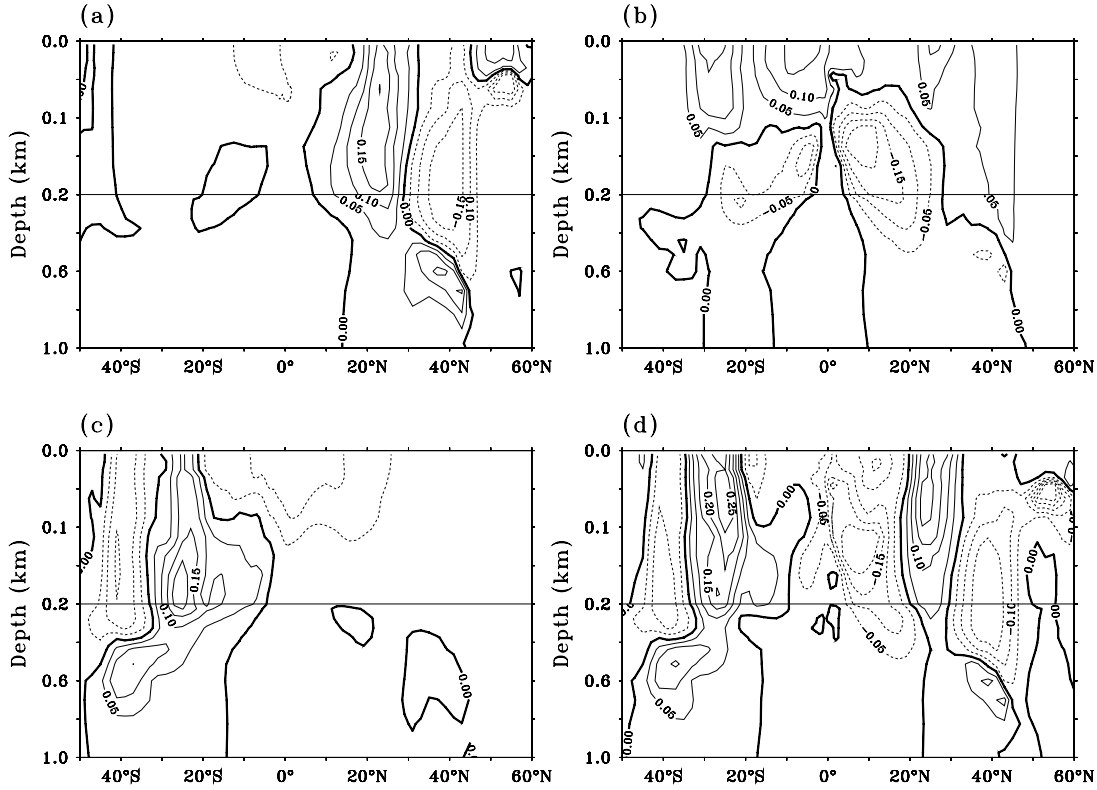

Figure 11. Time-averaged (1988 to 2000) and zonally averaged temperature anomalies in (a) NP, (b) EP, (c) SP, and (d) PTB. The contour interval is 0.05°C.

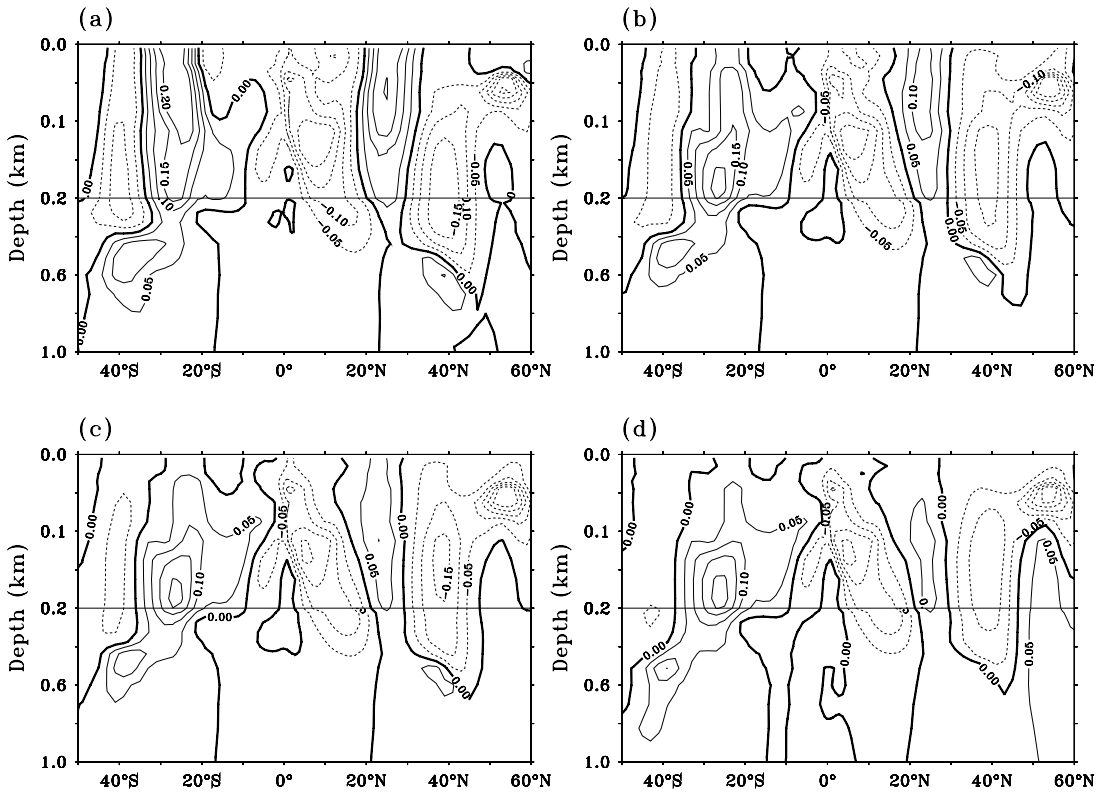

Figure 12. Time-averaged (1988 to 2000) and zonally averaged temperature anomalies in the Pacific with SST damping of (a) zero, (b) 8 Wm^{-2} K^{-1}, (c) 17 Wm^{-2} K^{-1}, and (d) 50 Wm^{-2} K^{-1}. The contour interval is 0.05°C.

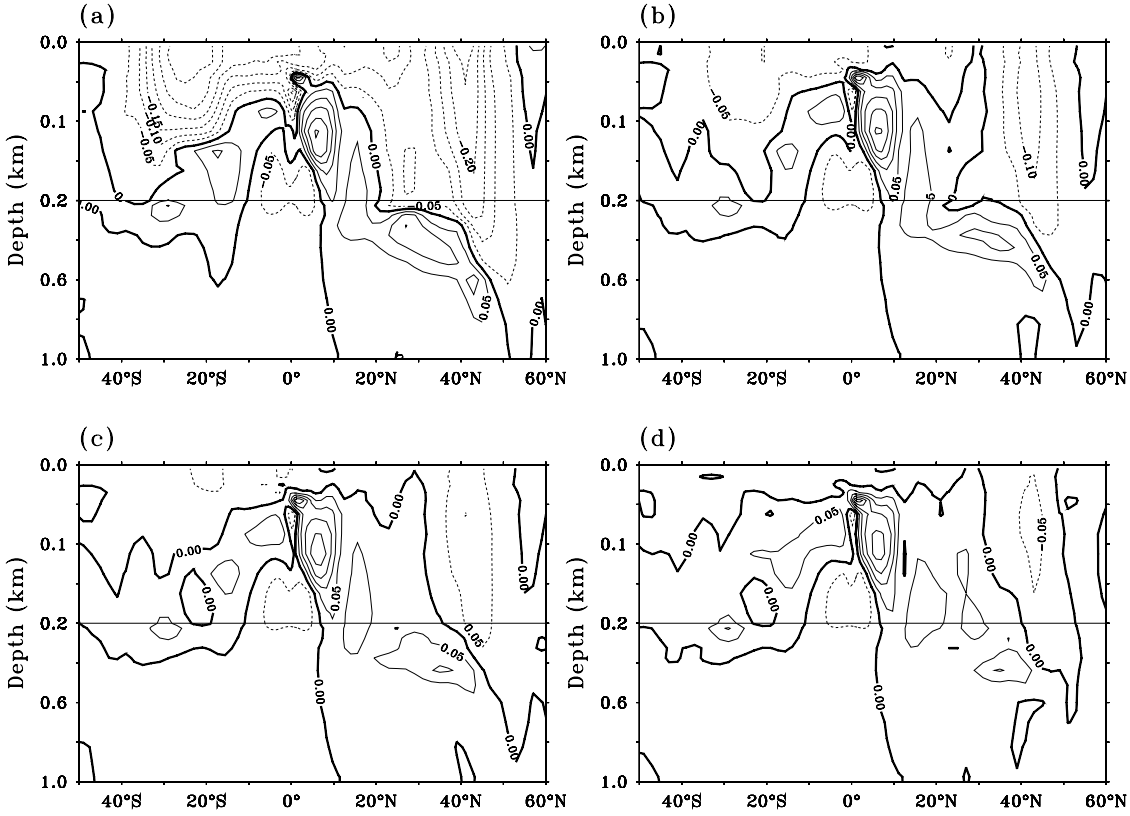

Figure 13. Same as Figure 12 except for the Atlantic Ocean.

itation) in the subtropical North and South Pacific and in the tropical Atlantic, and negative (more precipitation or less evaporation) in the tropical Pacific. Experiments showed that the spatial distribution of salinity anomalies was similar to that of anomalous EmP and that the salinity changes were as large as 0.8 psu. Because of large changes in salinity and therefore density, the subtropical gyres spun down in the Pacific and the SEC strengthened in the tropical Pacific. The spindown of the subtropical gyres and the strengthening of the SEC were directly driven by positive anomalous EmP in the subtropics and negative anomalous EmP in the tropics, which was consistent with the Goldsbrough-Stommel circulation hypothesis.

[35] Associated with these changes in ocean circulations, the western subtropics of the North and South Pacific cooled down owing to a reduced heat transport by a weaker Kuroshio and a weaker EAC. The eastern subtropics of the North and South Pacific warmed up owing to reduced cooling by weaker equatorward interior flows. The tropical Pacific cooled down owing to increased cooling by a stronger SEC. These results confirm that temperature changes may not result directly from local EmP forcing as also indicated by *Huang et al.* [2005]. For example, the positive anomalous EmP in the North and South Pacific can not only result in a warming and cooling in the subtropics, but also result in a cooling in the tropical Pacific; the negative anomalous EmP in the tropical Pacific can not only result in a warming in the tropics, but also result in a warming and cooling in the subtropical North and South Pacific. Ocean circulation changes also contributed to the cooling in the Atlantic, but the cooling largely resulted from stronger vertical mixing by denser surface water due to positive anomalous EmP.

[36] The surface flux boundary condition on model SST was used in our main experiments without considering any possible damping from the atmosphere owing to changes in air-sea heat flux. Additional simulations showed, however, that the surface flux boundary condition did not affect our conclusions significantly in the Pacific Ocean, since temperature anomalies were driven largely by anomalous ocean circulations which, in turn, were driven by anomalous EmP. Nevertheless, the atmospheric damping did weaken temperature anomalies in the Atlantic Ocean, since the anomalies were driven largely by vertical mixing which was directly associated with the surface temperature damping.

[37] It is important to note that the typical timescale of temperature variability due to anomalous EmP in the subtropical oceans was longer than 20 years in our experiments. Large temperature anomalies (1°C) at decadal and longer timescales indicated that the Pacific and Atlantic oceans were sensitive to the EmP variability, which has verified our hypothesis. This conclusion is consistent with the work of *Schneider and Barnett* [1995], *Anderson et al.* [1996], and *Feng et al.* [2000], who suggested that EmP is as important as surface heat flux in determining the upper-ocean buoyancy. The SST changes due to anomalous EmP in our experiments imply that the feedback of SST anomalies to the atmospheric circulation and precipitation may be significantly large, according to the studies by *Gill* [1980], *Trenberth and Hurrell* [1994], and *Graham* [1994]. This

may be a strong indication that EmP variability can play an important role in climate variability at interannual and longer timescales.

[38] Finally, the model resolution in the equatorial and western boundary regions in our experiments is relatively coarse so that equatorial currents (the South Equatorial Current and the Equatorial Undercurrent), the western boundary currents (the Gulf Stream and the Kuroshio), and the speed of Kelvin waves along the western boundary and the equator were much weaker than those in nature. Therefore their roles in affecting ocean temperature may still be underestimated by the MIT OGCM.

[39] **Acknowledgments.** The authors thank Andrew DeCandis for his help in preparing evaporation and precipitation data, Thierry Delcroix for providing observed SSS data, and Geoffrey Gebbie, Benny Cheng, Tony Lee, and Dimitris Menemenlis for their suggestions in setting up OGCM experiments. Constructive criticisms by James Richman and two anonymous reviewers are gratefully acknowledged. This research was supported by NASA grants NAG5-11785 and NAG5-12729. Center for Research on the Changing Earth System contribution 2.

References

Anderson, S. P., R. A. Weller, and R. B. Lukas (1996), Surface buoyancy forcing and the mixed layer of the western Pacific Warm Pool: Observations and 1D model results, *J. Clim.*, *9*, 3056–3085.

Bjerknes, J. (1969), Atmospheric teleconnections from the equatorial Pacific, *Mon. Weather Rev.*, *97*, 163–172.

Cayan, D. R. (1992), Latent and sensible heat flux anomalies over the northern oceans: The connection to monthly atmospheric circulation, *J. Clim.*, *5*, 354–369.

Chou, S.-H., C.-L. Shie, R. M. Atlas, and J. Ardizzone (1997), Air-sea fluxes retrieved from special sensor microwave imager data, *J. Geophys. Res.*, *102*, 12,705–12,726.

da Silva, A. M., C. C. Young, and S. Levitus (1994), *Atlas of Surface Maine Data 1994*, *NOAA Atlas NESDIS 6-8*, Natl. Oceanic and Atmos. Admin., Silver Spring, Md.

Delcroix, T., B. Dewitte, Y. du Penhoat, F. Masia, and J. Picaut (2000a), Equatorial waves and warm pool displacements during the 1992–1998 El Niño Southern Oscillation events: Observation and modeling, *J. Geophys. Res.*, *105*, 26,045–26,062.

Delcroix, T., C. Henin, F. Masia, and D. Varillon (2000b), *Three Decades of In Situ Sea Surface Salinity Measurements in the Tropical Pacific Ocean* [CD-ROM], Inst.de Rech. pour le Dev., Noumea, New Caledonia.

Deser, C., M. A. Alexander, and M. S. Timlin (1996), Upper ocean thermal variations in the North Pacific during 1970–1991, *J. Clim.*, *9*, 1840–1855.

Fedorov, A. V., R. C. Pacanowski, S. G. Philander, and G. Boccaletti (2004), The effect of salinity on the wind-driven circulation and the thermal structure of the upper ocean, *J. Phys. Oceanogr.*, *34*, 1949–1966.

Feng, M., R. Lukas, P. Hacker, R. A. Weller, and S. P. Anderson (2000), Upper-ocean heat and salt balances in the western equatorial Pacific in response to the intraseasonal oscillation during TOGA COARE, *J. Clim.*, *13*, 2409–2427.

Frankignoul, C., F. Bonjean, and G. Reverdin (1996), Interannual variability of surface currents in the tropical Pacific during 1987–1993, *J. Geophys. Res.*, *101*, 3629–3647.

Giese, B. S., and J. A. Carton (1999), Interannual and decadal variability in the tropical and midlatitude Pacific Ocean, *J. Clim.*, *12*, 3402–3418.

Gill, A. E. (1980), Some simple solution for heat induced tropical circulation, *Q. J. R. Meteorol. Soc.*, *106*, 447–462.

Goldsbrough, G. R. (1933), Ocean currents produced by evaporation and precipitation, *Proc. R. Soc. London, Ser. A*, *141*, 512–517.

Graham, N. E. (1994), Decadal-scale climate variability in the 1970s and 1980s: Observations and model results, *Clim. Dyn.*, *10*, 135–162.

Gu, D., and S. G. H. Philander (1997), Interdecadal climate fluctuations that depend on exchange between the tropics and extratropics, *Science*, *275*, 805–807.

Hellerman, S., and M. Rosenstein (1983), Normal monthly wind stress over the world ocean with error estimates, *J. Phys. Oceanogr.*, *13*, 1093–1104.

Henin, H., Y. du Penhoat, and M. Ioualalen (1998), Observations of sea surface salinity in the western Pacific fresh pool: Large-scale changes in 1992–1995, *J. Geophys. Res.*, *103*, 7523–7536.

Huang, B., and Z. Liu (2001), Temperature trend of the last 40 years in the upper Pacific Ocean, *J. Clim.*, *14*, 3738–3750.

Huang, B., and Z. Liu (2002), An OGCM simulation of seasonal and interannual variabilities in the surface-layer Pacific of the equatorial band, *Adv. Atmos. Sci.*, *19*, 219–235.

Huang, B., and V. M. Mehta (2004), The response of Indo-Pacific Warm Pool to interannual variations in net atmospheric freshwater, *J. Geophys. Res.*, *109*, C06022, doi:10.1029/2003JC002114.

Huang, B., P. H. Stone, A. P. Sokolov, and I. V. Kamenkovich (2003), Ocean heat uptake in transient climate change: Mechanisms and uncertainty due to subgrid-scale eddy mixing, *J. Clim.*, *16*, 3344–3356.

Huang, B., V. M. Mehta, and N. Schneider (2005), Oceanic response to idealized freshwater flux in the Pacific at decadal timescale, *J. Phys. Oceanogr.*, in press. (Available at http://www.crces.org/pubs.php)

Huang, R. X. (1993), Real freshwater flux as a natural boundary condition for the salinity balance and thermohaline circulation forced by evaporation and precipitation, *J. Phys. Oceanogr.*, *23*, 2428–2446.

Huffman, G. J., et al. (1997), The Global Precipitation Climatology Project (GPCP) Combined Precipitation Data Set, *Bull. Am. Meteorol. Soc.*, *78*, 5–20.

Jacobs, G. A., H. E. Hurlburt, J. C. Kindle, E. J. Metzer, J. L. Mitchell, W. J. Teague, and A. J. Walcraft (1994), Decadal-scale trans-Pacific propagation and warming effects of an El Niño, *Nature*, *370*, 360–363.

Jiang, S., P. H. Stone, and P. Malannotte-Rizzoli (1999), An assessment of the Geophysical Fluid Dynamics Laboratory ocean model with coarse resolution: Annual-mean climatology, *J. Geophys. Res.*, *104*, 25,623–25,645.

Large, W. G., J. C. McWilliams, and S. C. Doney (1994), Oceanic vertical mixing: A review and a model with non-local boundary layer parameterization, *Rev. Geophys.*, *32*, 363–403.

Latif, M., and T. Barnett (1994), Causes of decadal climate variability over the North Pacific and North America, *Science*, *266*, 634–637.

Latif, M., and T. Barnett (1996), Decadal climate variability over the North Pacific and North America: Dynamics and predictability, *J. Clim.*, *9*, 2407–2434.

Lau, N. C., and M. J. Nath (1996), The role of the atmospheric bridge in linking tropical Pacific ENSO events to extratropical SST anomalies, *J. Clim.*, *9*, 2036–2057.

Levitus, S., and T. Boyer (1994), *World Ocean Atlas 1994*, vol. 4, *Temperature*, *NOAA Atlas NESDIS 4*, Natl. Oceanic and Atmos. Admin., Silver Spring, Md.

Levitus, S., R. Burgett, and T. Boyer (1994), *World Ocean Atlas 1994*, vol. 3, *Nutrients*, *NOAA Atlas NESDIS 3*, Natl. Oceanic and Atmos. Admin., Silver Spring, Md.

Liu, Z., and B. Huang (1997), A coupled theory of tropical climatology: Warm pool, cold tongue, and Walker Circulation, *J. Clim.*, *10*, 1662–1679.

Lysne, J., P. Chang, and B. S. Giese (1997), Impact of the extratropical Pacific on equatorial variability, *Geophys. Res. Lett.*, *24*, 2589–2592.

Marshall, J., A. Adcroft, C. Hill, L. Perelman, and C. Heisey (1997), A finite volume, incompressible Navier-Stokes model for studies of the ocean on parallel computers, *J. Geophys. Res.*, *102*, 5753–5766.

Masuda, S. (2002), Role of the ocean in the decadal climate change in the North Pacific, *J. Geophys. Res.*, *107*(C12), 3224, doi:10.1029/2002JC001420.

Matsuukra, T., and S. Iizuka (2000), Zonal migration of the Pacific warm-pool tongue during El Niño events, *J. Phys. Oceanogr.*, *10*, 1582–1600.

Miller, A. J., D. R. Cayan, T. P. Barnett, N. E. Graham, and J. M. Oberhuber (1994), Interdecadal variability of the Pacific Ocean: Model response to observed heat flux and wind stress anomalies, *Clim. Dyn.*, *9*, 287–302.

Murtugudde, R., and A. J. Bussalacchi (1998), Salinity effects in a tropical ocean model, *J. Geophys. Res.*, *103*, 3283–3300.

Perigaud, C., J. P. McCreary, and K. Q. Zhang (2003), Impact of interannual rainfall anomalies on Indian Ocean salinity and temperature variability, *J. Geophys. Res.*, *108*(C10), 3319, doi:10.1029/2002JC001699.

Philander, S. G. (1990), *El Niño, La Niña, and the Southern Oscillation*, 293 pp., Elsevier, New York.

Schneider, N. (2000), A decadal spiciness mode in the tropics, *Geophys. Res. Lett.*, *27*, 257–260.

Schneider, N., and T. Barnett (1995), The competition of freshwater and radiation in forcing the ocean during El Niño, *J. Clim.*, *8*, 980–992.

Shapiro, R. (1970), Smoothing, filtering, and boundary effects, *Rev. Geophys.*, *8*, 359–387.

Stommel, H. M. (1984), The delicate interplay between wind-stress and buoyancy input in ocean circulation: The Goldsbrough variation, *Tellus, Ser. A*, *46*, 111–119.

Trenberth, K. E., and J. W. Hurrell (1994), Decadal atmosphere-ocean variations in the Pacific, *Clim. Dyn.*, *9*, 303–319.

Vialard, J., and P. Delecluse (1998a), An OGCM study for the TOGA decade: Part I. Role of salinity in the physics of the western Pacific Fresh Pool, *J. Phys. Oceanogr.*, *28*, 1071–1088.

Vialard, J., and P. Delecluse (1998b), An OGCM study for the TOGA decade: Part II. Barrier-layer formation and variability, *J. Phys. Oceanogr.*, *28*, 1089–1106.

Walker, G. T. (1924), Correlation in seasonal variations of weather: IX. A further study of world weather, *Mem. Ind. Meteorol. Dep.*, *24*, 275–332.

White, W. B., and T. P. Barnett (1972), A servomechanism in the ocean/atmosphere system of the mid-latitude North Pacific, *J. Phys. Oceanogr.*, *2*, 372–381.

Yang, S., K.-M. Lau, and P. S. Schopf (1999), Sensitivity of the tropical Pacific Ocean to precipitation-induced freshwater flux, *Clim. Dyn.*, *15*, 737–750.

B. Huang and V. M. Mehta, Center for Research on the Changing Earth System (CRCES), 10211 Wincopin Circle, Suite 240, Columbia, MD 21044, USA. (byh@crces.org)

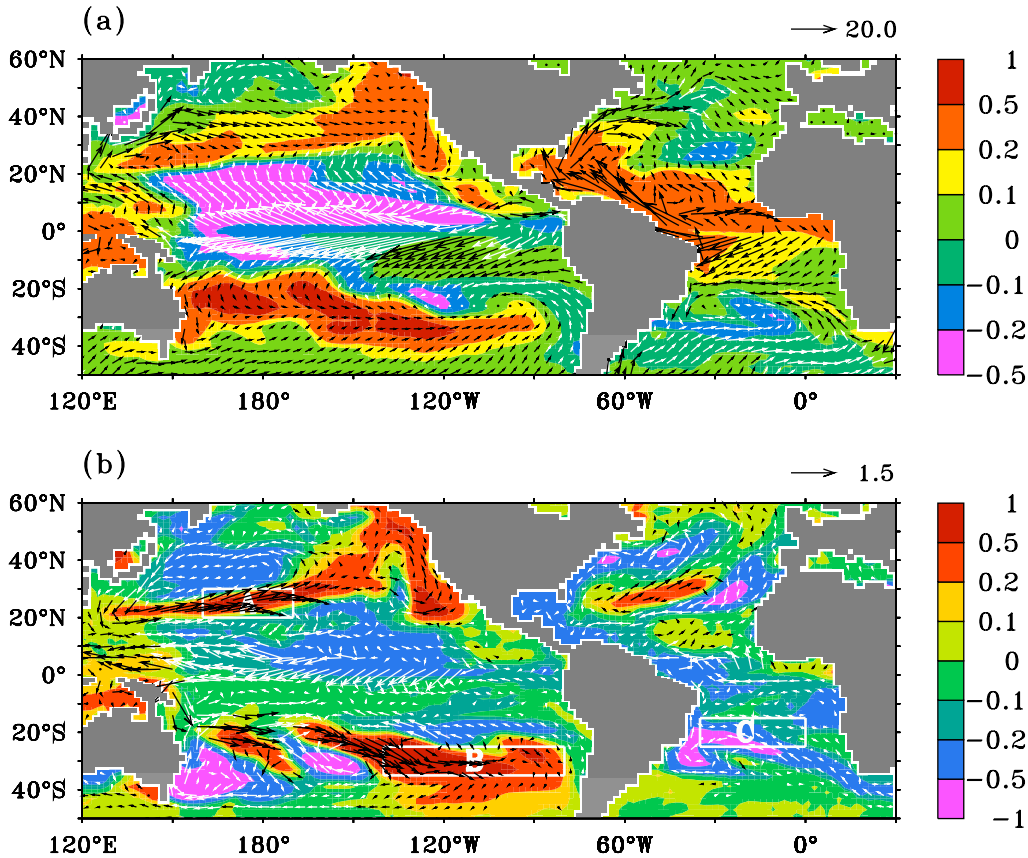

Figure 3. (a) Averaged (1988 to 2000) near-surface (0 to 50 m) salinity anomaly (shaded, °C) between PTB and CTR, and average currents (vector, 20 cm s^{-1}) in PTB. (b) Average near-surface (0 to 50 m) temperature (shaded) and current (vector, 1.5 cm s^{-1}) anomalies between PTB and CTR. Vector colors are changed to increase contrast with background shading. Vectors are shown on 4° longitude and 4° latitude grids. Regions A, B, and C are shown as rectangular boxes.

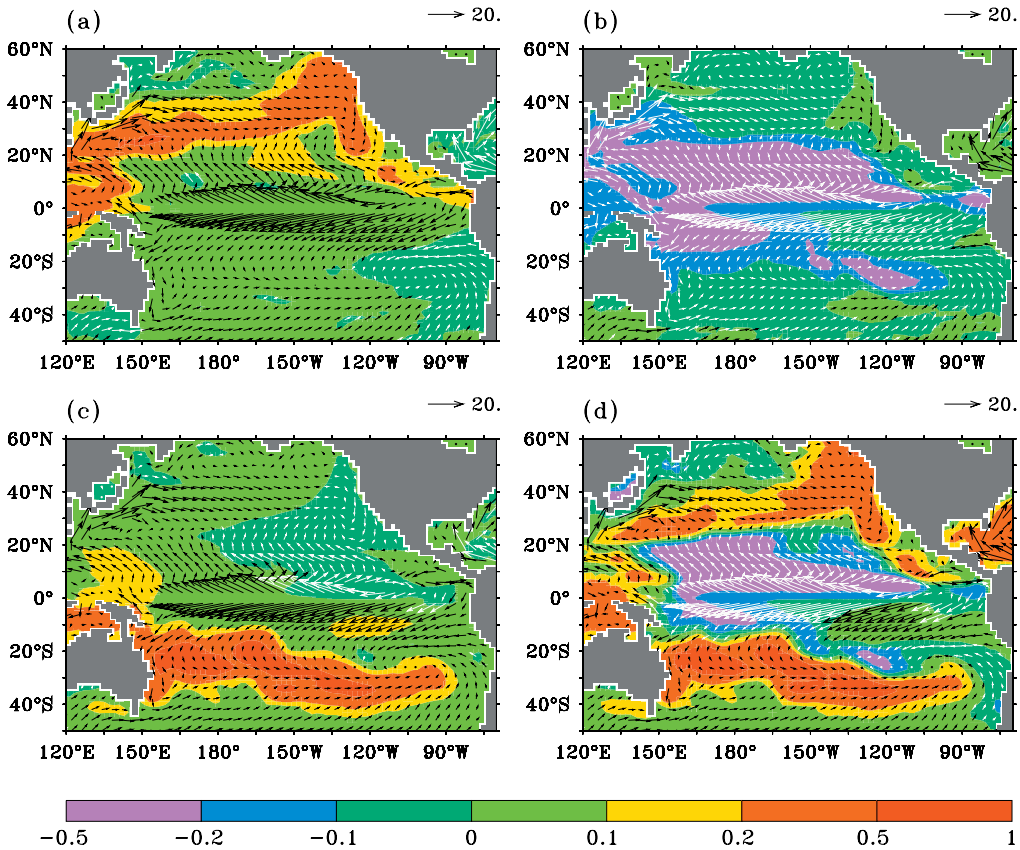

Figure 9. Averaged (1988 to 2000) near-surface (0 to 50 m) salinity anomalies (shaded, psu) and average currents (vector, 20 cm s^{-1}) in (a) NP, (b) EP, (c) SP, and (d) PTB. Vector colors are changed to increase contrast with background shading. Vectors are shown on a 4° longitude × 4° latitude grid.

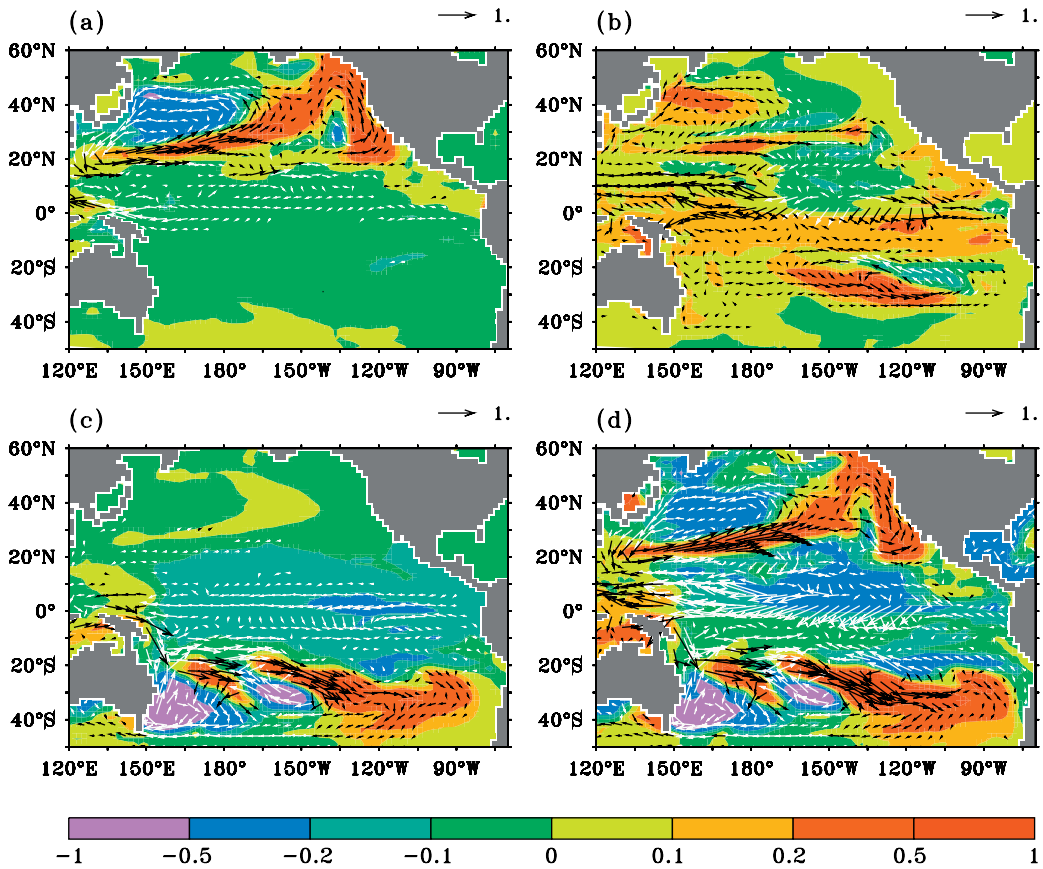

Figure 10. Averaged (1988 to 2000) near-surface (0 to 50 m) temperature (shaded, psu) and current (vector, 1 cm s^{-1}) anomalies in (a) NP, (b) EP, (c) SP, and (d) PTB. Vector colors are changed to increase contrast with background shading. Vectors are shown on a 4° longitude × 4° latitude grid.